Comparative Analyses of Physically Based Snowmelt Models for Climate Simulations

J. JIN

LASG, Institute of Atmospheric Physics, CAS, Beijing, China

X. GAO, Z.-L. YANG, R. C. BALES, S. SOROOSHIAN, AND R. E. DICKINSON

Department of Hydrology and Water Resources, The University of Arizona, Tucson, Arizona

S. F. SUN AND G. X. WU

LASG, Institute of Atmospheric Physics, CAS, Beijing, China

(Manuscript received 8 June 1998, in final form 23 September 1998)

ABSTRACT

A comparative study of three snow models with different complexities was carried out to assess how a physically detailed snow model can improve snow modeling within general circulation models. The three models were (a) the U.S. Army Cold Regions Research and Engineering Laboratory Model (SNTHERM), which uses the mixture theory to simulate multiphase water and energy transfer processes in snow layers; (b) a simplified three-layer model, Snow–Atmosphere–Soil Transfer (SAST), which includes only the ice and liquid-water phases; and (c) the snow submodel of the Biosphere–Atmosphere Transfer Scheme (BATS), which calculates snowmelt from the energy budget and snow temperature by the force–restore method. Given the same initial conditions and forcing of atmosphere and radiation, these three models simulated time series of snow water equivalent, surface temperature, and fluxes very well, with SNTHERM giving the best match with observations and SAST simulation being close. BATS captured the major processes in the upper portion of a snowpack where solar radiation provides the main energy source and gave satisfying results for seasonal periods. Some biases occurred in BATS surface temperature and energy exchange due to its neglecting of liquid water and underestimating snow density. Ice heat conduction, meltwater heat transport, and the melt–freeze process of snow exhibit strong diurnal variations and large gradients at the uppermost layers of snowpacks. Using two layers in the upper 20 cm and one deeper layer at the bottom to simulate the multiphase snowmelt processes, SAST closely approximated the performance of SNTHERM with computational requirements comparable to those of BATS.

1. Introduction

One of the primary functions of snow cover in GCMs is to control energy and water exchanges with the atmosphere through its influence on surface temperature and albedo. While albedo is determined locally by near-surface grain sizes, deposition of particulates, and the presence of water in the snowpack, surface temperature is determined by the energy balance at the uppermost layers, most notably freezing and thawing. Because the diurnal and seasonal timescales are both important for climate modeling, a good snow model must be able to capture these two scales. Because of the importance of snow in simulating climate, significant progress has been made to better represent snow cover in GCMs (Dickinson et al. 1986; Sellers et al. 1986; Verseghy 1991; Loth et al. 1993; Marshall et al. 1994; Lynch-Stieglitz 1994; Douville et al. 1995; Pollard and Thompson 1995; Bonan 1996; Walland and Simmonds 1996). In the early versions of GCM snow models, diurnal variations were treated by including a layer of approximately the diurnal penetration depth, that is, about 0.1 m, using some variation on the force-restore method (Dickinson 1988). Over a season, penetration depth is on the order of a few meters; if such depths are achieved, the corresponding heat flux to the bottom of the snow is negligibly small. Furthermore, as seasonal snow is accumulated on timescales of days to months, the temperature profile deep beneath the surface can be expected to change slowly and be in approximately steady state. Hence, the deep snow could be represented by a single slab. For climate modeling, the most important snow densities to model correctly (to be realistic thermal fluxes) are those of the top layers. The deep snow slab is characterized primarily by its water content, but some idea of snow density is also needed in order to validate

Corresponding author address: J. Jin, Department of Hydrology and Water Resources, The University of Arizona, Building 11, P.O. Box 210011, Tucson, AZ 85721-0011.
E-mail: jjm@hwr.arizona.edu

against observed snow depths and to get the steady-state fluxes to the underlying soil layers. In addition, heterogeneity across the landscape can be important for both albedo and conductive and atmospheric flux transfers.

From the climate viewpoint, the most crucial time for snow modeling is during the spring snowmelt period. This same period is also critical from the hydrologic viewpoint. Over this period, solar fluxes are large, and albedo variations have a major effect; at the same time, removal of the snow can drastically change surface albedos. Further, the timing of snowmelt is a major influence on the timing of water removal by runoff. The spring snowmelt period, besides its importance, has other unique features that influence the modeling approach. A better description of this spring snowmelt period could contribute substantially to understanding the relationships between snow cover, atmospheric processes, and surface energy and water budgets during normal and anomalous snow cover regimes (Yeh et al. 1983; Barnett et al. 1989; Yasunari et al. 1991; Cess et al. 1991; Wu et al. 1995; Houghton et al. 1996; Walland and Simmonds 1997; Leese 1997).

Despite offline evaluations of the GCM snow submodels against field data (e.g., Yang et al. 1997) and those examining the performances of snow models in GCMs (e.g., Foster et al. 1996), there has been little work that provides an understanding of the relationship between model performances and model physical structures. This paper intends to fill this gap by examining three snow models spanning a range of complexity against the field data from Mammoth Mountain, California (Harrington and Bales 1998). These three models include the detailed process-oriented model of Jordan (1991), a three-layer snow model (the Snow–Atmosphere–Soil Transfer Model, SAST) with simplified treatment of snow processes (Sun and Jin 1998), and a Biosphere–Atmosphere Transfer Scheme (BATS) snow submodel of Dickinson et al. (1993), which is specifically designed for use in GCMs. This paper addresses the following questions: (a) How accurate are these models over both seasonal and diurnal periods when the models are driven by the same initial conditions and atmospheric forcing variables? (b) What are the differences in the models' accuracy, and how do they relate to the key snowmelt processes that are described or neglected by these models? (c) What are the diurnal and vertical variations of snowpacks during melt seasons that are most relevant to snow surface energy exchanges, and how can this knowledge be applied to a simple snowmelt model for incorporation into GCMs?

2. Data

Automatic snow and meteorological measurements have been made at Mammoth Mountain in the eastern Sierra Nevada, California, since 1987, including automatically recorded meteorological variables, lysimeter measurements, and snow pit measurements (Harrington and Bales 1998). Lysimeter and pit data were taken from two sites (north and south), which are about 20 m apart and have different snow depths. The measured meteorological variables include wind speed, air temperature, relative humidity, and net solar and downward longwave radiation at 15-min intervals. Two clusters of 1 m $\times$ 1 m lysimeters ($\sim$20 cm apart) are installed at the base of the snowpack at both north and south sites to measure the meltwater discharge every half-hour. Biweekly, two snow pits excavated from the sites provide snow depth, snow water equivalent (SWE), and vertical profiles of snow density and temperature at 0.1-m resolution.

3. Models

The one-dimensional U.S. Army Cold Regions Research and Engineering Laboratory Model (SNTHERM) was developed for predicting properties and processes within strata of snow and frozen soil. The model uses mixture theory to describe the dynamic and thermal processes of five mixture constituents: dry air, dry soil, and the three phases of water. Snowmelt is assumed to drain by gravity, and water vapor is assumed to move along the temperature gradient. Water and energy exchanges at the surface and bottom of a snowpack and internal snow processes such as ice grain growth, snow ablation, densification, and metamorphosis are modeled through the numerical solution of mass and heat-transfer equations. To simulate such detailed physics, SNTHERM uses a large number of snow layers and executes calculations at short time steps (5–900 s). Because vegetation influences and spatial distribution of snow are not considered in SNTHERM, the model conceptually applies to snowpacks overlying bare soil.

Compared to SNTHERM, the BATS snow submodel (Dickinson et al. 1993; Yang et al. 1997) is a greatly simplified approach designed for use in GCMs that focus on long-term climate. In BATS, snow is lumped into a single uniform layer that lies over homogeneous soil, and the extended force-restore method (Dickinson 1988) is used to calculate the surface temperature (at the depth subject to diurnal variation) and subsurface temperature (at the depth subject to seasonal variation) for the composite snow and soil layer. Snowmelt is estimated using an energy balance for the surface snow. Internal radiative and thermodynamic snowpack processes are omitted; key snowpack properties such as surface albedo, ice-grain size, and snow density are parameterized as functions of surface snow age. Vegetation effects on snow cover and subgrid snow fractional coverage over various land surface types are modeled in order to realistically represent the snow processes over a large-scale ($\sim 1^\circ \times 1^\circ$) grid.

The SAST model (Sun et al. 1999; Jin et al. 1999) is one of multiple efforts to simplify SNTHERM to a point where it can be used to describe the variation of snow cover for a wide region, especially for both long-

TABLE 1. Comparison of several snow models for use in GCMs.

Model developer name/host GCM	Physical equations	Water phases	Layering	Liquid water treatment	Snow density
Jordan (1991) SNTHERM/No GCM (USA)	Energy-mass balance	Ice Liquid water Vapor	Multilayers	Gravitational flow	Function of mass balance and compaction
Loth et al. (1993)/ ECHAM (Germany)	Energy-mass balance	Ice Liquid water Vapor Dry air	2–5 layers	Liquid water–holding capacity as function of snow density	Function of mass balance and compaction
Sun and Jin (1999) SAST/GOALS (China)	Energy-mass balance	Ice Liquid water	3 layers	Liquid water–holding capacity as function of snow density	Function of mass balance and compaction
Lynch-Stieglitz (1994) GISS-LS/GISS (USA)	Energy-mass balance	Ice Liquid water	3 layers	Constant liquid water–holding capacity	Function of snow age
Verseghy (1991) CLASS/CCC (Canada)	Surface energy balance for snowmelt Mass balance for SWE change Energy balance for no-melting temperature	Ice Liquid water	1 layer	Constant liquid water–holding capacity	Function of snow age
Bonan (1996) LSM/ CCM3 (USA)	Surface energy balance for snowmelt Mass balance for SWE change Energy balance for no-melting temperature	Ice	1 layer	No	Constant
Dickinson et al. (1993), BATS/CCM2,3 (USA) Sellers et al. (1986) SiB/ CSU (USA) Pitman et al. (1991) BEST/BMRC (Australia)	Surface energy balance for snowmelt Mass balance for SWE change Force-restore for no-melting temperature	Ice	2 snow–soil composite layers	No	Function of snow age in BATS/BEST Constant in SiB

term and short-term atmosphere modeling (Loth et al. 1993; Lynch-Stieglitz 1994). In the model, the dry air and water vapor components in a snowpack are neglected. The gravitational flow of meltwater is replaced by the concept of water-holding capacity: meltwater in a layer will remain there until it exceeds the layer's holding capacity; after that, the excess is delivered to the lower layer. With both ice and liquid-water phases in a snowpack, the three snow compaction processes of SNTHERM (metamorphism, weight, and melting–refreezing) are retained in SAST to simulate the variability of snow density. Because SAST neglects the vapor phase, ice-grain size is parameterized as a function of snow density. In SAST, only three layers are used to describe a snowpack. The top two layers are within 20 cm below the snow surface to simulate the density and temperature gradients and snowmelt; the third layer represents the remaining body of the snowpack. When solving the energy equation, SAST uses heat content as a prognostic variable instead of snow temperature. By assuming that 0°C water possesses zero heat content, this approach can simplify the representation of meltwater and treat the melting and refreezing process easily. The same approach was employed by Lynch-Stieglitz (1994) and Tarboton and Luce (1996).

In Table 1, SNTHERM is compared with six snow models that have been used in GCM land surface schemes. Models are listed in order of complexity. SNTHERM provides the most complete property and process simulations of snow physics, whereas the BATS snow submodel represents the sort of relatively simple snow model that has been widely used in GCMs. The remaining four models have incorporated factors found in SNTHERM but not in BATS: 1) use of separate snow and soil models instead of the snow–soil composite modeling in the force-restore approach; 2) improved parameterization of snow properties, especially relating snow density to various compaction mechanisms; 3) describing the influences of the liquid phase and phase changes on snow properties and processes, meanwhile using the concept of liquid-water-holding capacity to simplify the simulation of water flow; and 4) use of limited snow layers to reduce the model bias caused by the great variation in temperature and density along snow depth (especially for thick snowpacks in the nighttime). We thus select SNTHERM, SAST, and BATS as representative snow models for this study.

4. Methods

The same observed initial conditions and common parameters (Table 2), time-varying meteorological forcing, and atmospheric boundary layer stability schemes were applied to the three models (i.e., test in offline

TABLE 2. Common parameters for SNTHERM, SAST, and BATS.

Parameters	Value
Snow surface roughness (m)	0.002
Prantl number	1.0
Schmidt number	1.0
Soil porosity	0.40
Initial grain diameter (mm)	0.5*
Near-infrared extinction coefficient	400.0*
Reference height of meteorological data (m)	6.5

* For SNTHERM and SAST.

mode). To ensure that model performance was not influenced by the difference in absorbed radiation, the same observed net solar radiation and downward longwave radiation were employed for each model instead of calculating net radiation using their albedo schemes. The time interval of meteorological forcing was 30 min for SAST and BATS, but 15 min for SNTHERM. Because the snowpacks in this study overlaid bare soil, vegetation influences considered in BATS and SAST were neglected (vegetation fractional coverage equal to zero). Both SNTHERM and SAST include soil models, and BATS simulates the snow–soil composite without explicit description for the snow–soil interface; therefore, no boundary condition at the bottom of a snowpack was applied.

Four simulations for 1992 and 1993 at both north and south observation sites of Mammoth Mountain were conducted. Because of the close proximity (20 m) of these two sites, the same meteorological forcing was used, but they had different snow depth and initial conditions.

Both the BATS and SAST models have been applied to several datasets that cover entire seasonal cycles, such as the Russian and France data (Yang et al. 1997; Sun et al. 1999), but the Mammoth Mountain data are more appropriate for this analysis because their unique persistent measurements of variability in snow density and liquid water discharge can be used to gain insight into snowpack physical processes during the ablation period.

Because a snow model within a GCM must consider both the accumulation and ablation seasons, the ablation period was the main focus in this study for two reasons. First, the primary objective was to examine how well the models represent snowpack internal processes, such as ablation, sublimation, and compaction. The models were driven by observed meteorological data with weather-defined processes, such as snowfall and snowpack growth, prescribed. In the snow accumulation season, which has relatively low solar radiation and cold air temperature, internal processes are weak and accumulation becomes the major snowpack process (snow redistribution by wind is not simulated in these models). Second, the Project for Intercomparison of Land-Surface Parameterization Schemes (PILPS) simulations using 21 snow models driven by identical meteorological data from Valdai, Russia (Fig. 1), show that variations between models are relatively small during the snow accumulation season (November–March), but are much larger during the snowmelt season (March–May). In a snow model, accumulation is due to the snowfall and loss is mainly by snowmelt. In the Valdai simulations, sublimation averaged less than 4 mm day^{-1} (Schlosser et al. 1999). Thus, the main differences among the 21 models are in how they simulate internal snowpack processes during snowmelt. Because some of these same internal processes drive the (much smaller) accumulation season differences between models, results from our analysis should apply to the entire snow season.

5. Results

a. Seasonal variations of snowmelt

Six physical variables, that is, snow depth, SWE, snow surface temperature, meltwater efflux, and snow surface sensible and latent heat fluxes, were used to show the seasonal characteristics of snowmelt. Daily means of both modeled and observed values of these six variables for the north site during the 1993 snowmelt season are illustrated in Figs. 2 and 3, with statistics for the results summarized in Table 3.

The snow depth and SWE time series (Figs. 2a,b) simulated by the three models closely matched the observation. Because of the limited observation frequency, the comparisons were carried out between SAST or BATS and SNTHERM, which showed overall better performance against the field data than did the other two models. The root-mean-square difference (rmsd) of SWE was 0.038 m for SAST and 0.110 m for BATS (Table 3). BATS showed thicker snow depth {bias = 0.36 m, due mainly to the snow density parameterization [see section 5b(3)]} and longer snowmelt duration (~5 days). From Fig. 2b, note that the SWE in BATS was lower in the early period [day of year (DOY) 109–139] and then higher in the later period (after DOY 139) than those of SNTHERM and SAST. This early period difference occurs because, in BATS, the snowpack does not retain liquid water. Once an amount of snow melts, water immediately drains out of the snowpack, but in SNTHERM and SAST, the snowpack's liquid-water-holding capability delays initial release of meltwater. After the accumulation of meltwater exceeds the water-holding capability, meltwater will drain out as in BATS. The higher SWE values of BATS during the later period indicate a slower melting rate as compared to the other two models.

Simulated meltwater effluxes showed a similar temporal variation pattern as that observed, but had more than 12 days difference in duration (Fig. 2c). The onset of discharge started on the first day of snowmelt (DOY 109) for BATS, about 12 days later for SNTHERM, and 15 days later for SAST. During the period of snowmelt, water effluxes in BATS were consistently lower than

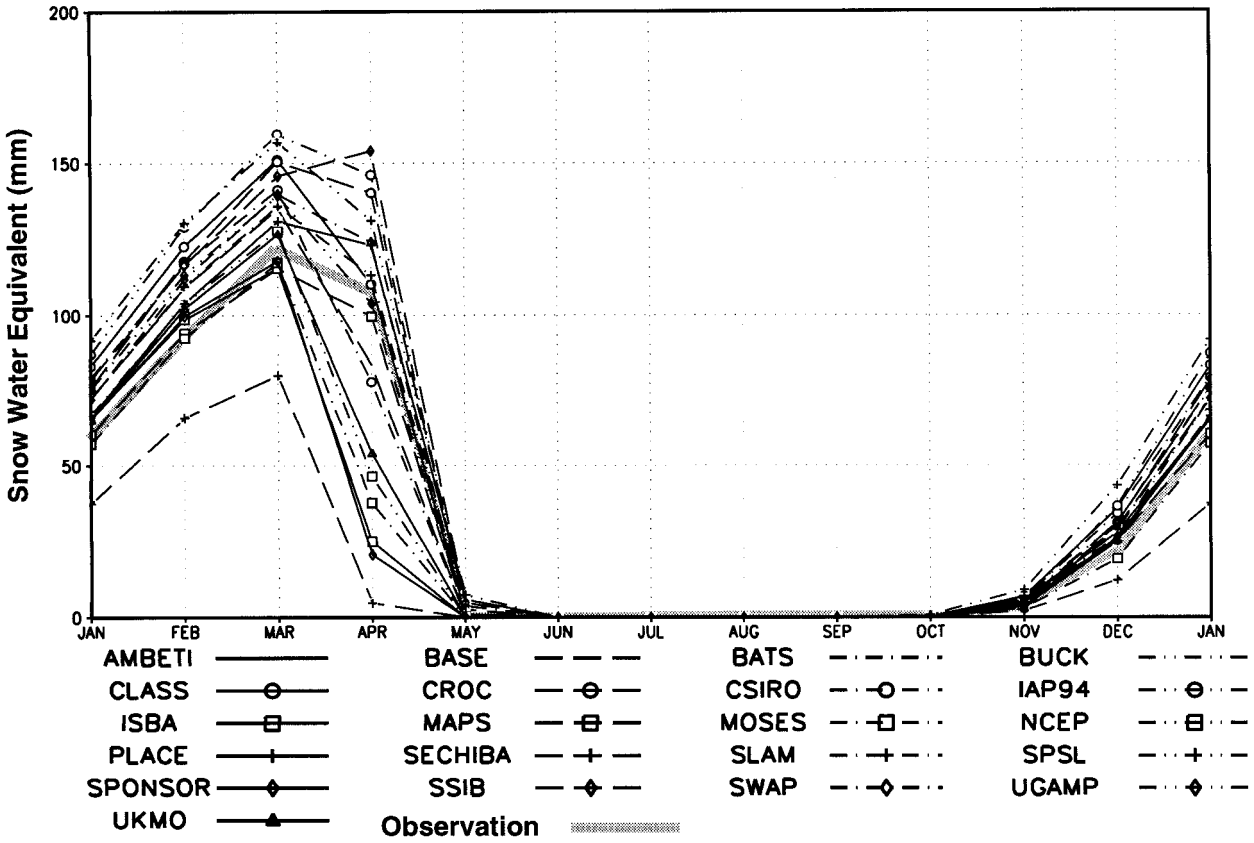

FIG. 1. Eighteen-year averaged seasonal cycles of snow water equivalent at Valdai, Russia, from observation and simulations (Schlosser et al. 1999; reproduced with permission).

those in the other two models due to its lower melt rate. The snowmelt ended first in SAST, on DOY 175, 3 days later in SNTHERM, and 8 days later in BATS. Because of the uncertainty in discharge measurements due to spatial variability (Harrington and Bales 1998), the lysimeter data were not used to quantitatively evaluate the accuracy of different models.

There were no significant differences in the simulated daily mean snow temperature for the three models (Fig. 2d). Unfortunately, there were no observations for comparison. The correlation coefficient and rmsd (Table 3) of surface temperature were 0.97 and 1.24 K for SAST, and 0.83 and 2.85 K for BATS, respectively, which indicates that the surface temperature of SAST was closer to SNTHERM's than that of BATS. From Table 3, small but consistently low biases in snow surface temperature were found in BATS in the four simulation cases (average ~ -0.72 K); this could be explained by the diurnal variability of snow surface temperature [see sections 5b(2) and 5b(4)].

Seasonal variations of various surface energy fluxes are illustrated in Figs. 3a–d. The net solar radiation was estimated from observations, with all other heat fluxes simulated by the models. The net solar radiation (mean value ~ -61 W m^{-2}) (Fig. 3a) and sensible heat flux (mean value ~ -60 W m^{-2}) (Fig. 3c) had consistently negative values (downward, warming the snow) during the melt season. In contrast, the net longwave radiation (mean value ~ 49 W m^{-2}) (Fig. 3b) always cooled the snow surface (positive values, upward), even though air temperature was higher than snow surface temperature, because the atmospheric emissivity of the atmosphere was lower than that of the snow surface. Figure 3d shows that the direction of the latent heat flux (mean value ~ 6 W m^{-2}) shifted frequently between snow-to-atmosphere (evaporation) and atmosphere-to-snow (condensation). From the mean values of the components of energy fluxes, the longwave radiation, sensible heat flux, and latent heat flux were approximately balanced ($49 - 60 + 6 = -5$ W m^{-2}), while the mean value of energy expended on snowmelt (~ -66 W m^{-2}) was almost equal to the solar radiation (~ -61 W m^{-2}), which indicates that solar radiation was the major energy source for snowmelt. The characteristics of energy exchange over the snow surface are distinguished from those of no-snow land surface. In fact, snow cover turned the function of land surface from a turbulent energy source (upward evaporation plays the major role) to a turbulent energy sink (downward sensible heat flux plays the major role) for the atmosphere boundary layer.

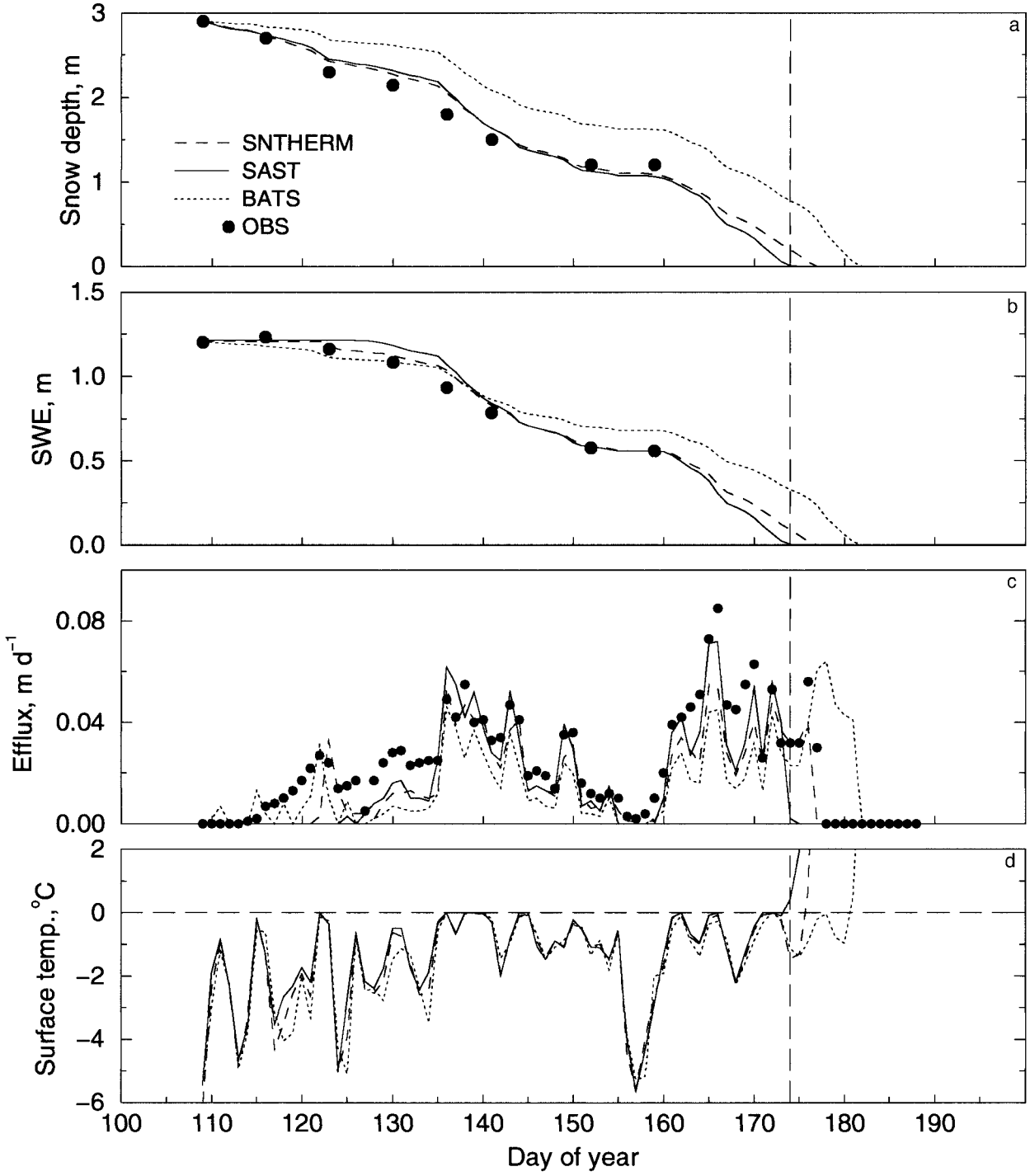

FIG. 2. Seasonal variation (at daily mean resolution) simulated by SNTHERM, SAST, and BATS at the north site in 1993 for (a) snow depth, (b) snow water equivalent, (c) meltwater efflux, and (d) surface temperature. The vertical dashed line for DOY 174 is when the snow was completely melted in the SAST simulation (DOY for day of year).

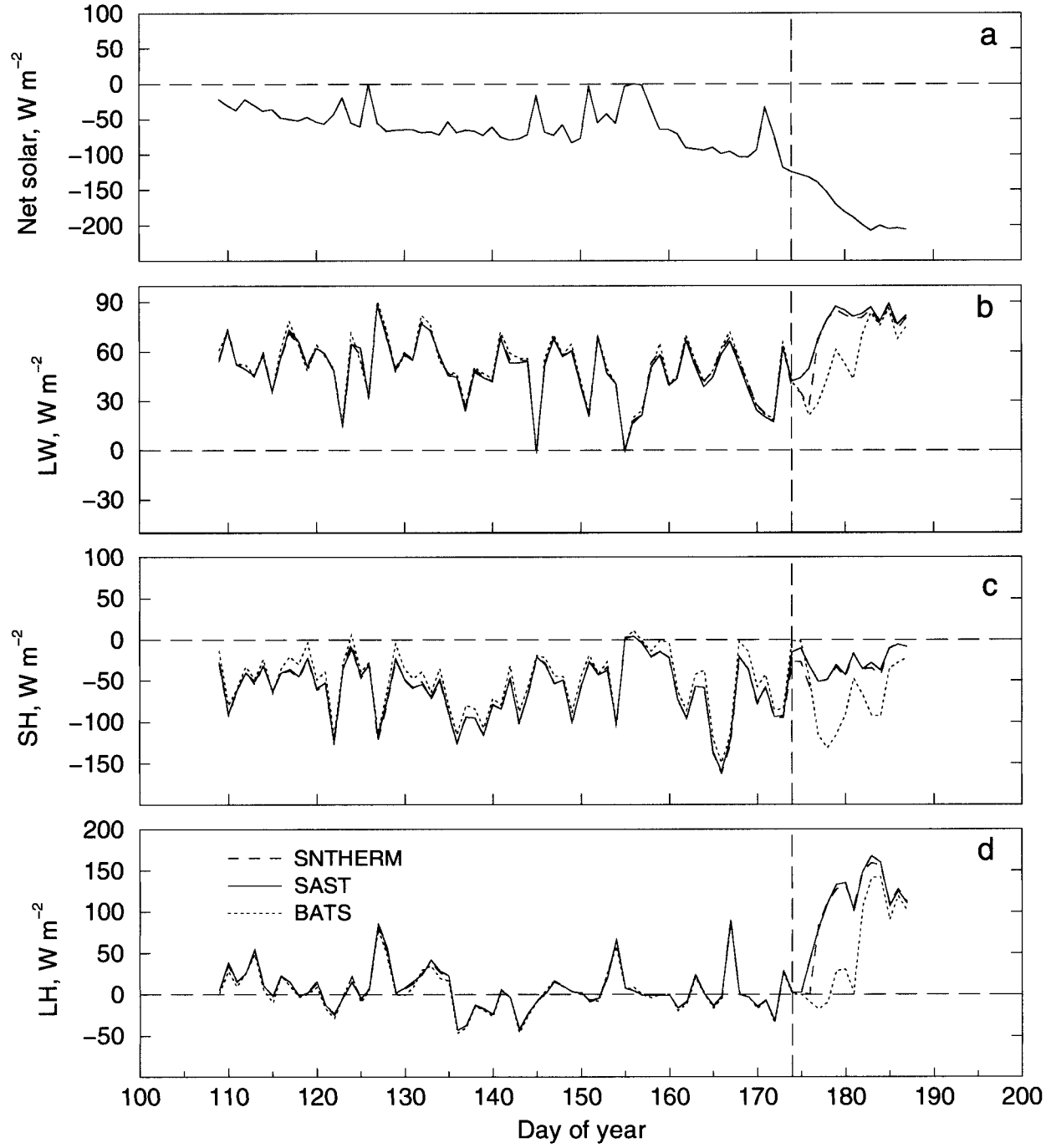

FIG. 3. The same as in Fig. 2 for (a) net solar radiation, (b) net longwave radiation, (c) sensible heat flux, and (d) latent heat flux.

This phenomenon can be seen from Figs. 3c–d during DOY 175–183. The modeled surface fluxes showed remarkable differences between SNTHERM or SAST and BATS, because, during this period, snow cover had disappeared in SAST and SNTHERM, but was still present in BATS.

b. Diurnal and vertical variations of snowmelt

1) STABILITY SCHEME OF THE ATMOSPHERE BOUNDARY LAYER OVER SNOW

To provide identical atmospheric conditions for the three models, the BATS calculation of the drag coef-

TABLE 3. Statistics of 1992–93 simulations at the Mammoth Mountain sites (R: root-mean-square difference, B: Bias, and C: correlation coefficient).

		1992						1993					
		North			South			North			South		
		R	B	C	R	B	C	R	B	C	R	B	C
Snow depth	SAST	0.12	−0.08	0.98	0.04	−0.02	0.99	0.06	−0.02	0.99	0.08	−0.06	0.99
	BATS	0.13	0.10	0.98	0.22	0.19	0.99	0.41	0.36	0.97	0.61	0.57	0.99
Snow water equivalent	SAST	0.08	−0.06	0.97	0.02	−0.00	0.99	0.04	0.00	0.99	0.07	0.04	0.99
	BATS	0.06	0.03	0.97	0.08	0.04	0.98	0.11	0.06	0.98	0.10	−0.09	0.99
Water efflux	SAST	0.03	−0.00	0.39	0.03	0.00	0.65	0.03	0.00	0.55	0.04	0.00	0.63
	BATS	0.02	0.00	0.54	0.03	0.00	0.54	0.03	−0.00	0.46	0.03	−0.00	0.64
Surface temperature	SAST	2.19	0.23	0.92	1.42	0.40	0.95	1.24	0.30	0.97	0.99	0.02	0.95
	BATS	3.15	−0.95	0.82	3.43	−0.86	0.66	2.85	−0.81	0.83	1.47	−0.25	0.89
Sensible heat flux	SAST	34.16	−0.24	0.91	7.63	1.48	0.99	6.56	1.43	0.99	18.21	2.22	0.98
	BATS	26.23	4.38	0.88	25.39	8.00	0.91	28.54	3.33	0.89	24.29	−5.77	0.98
Latent heat flux	SAST	25.36	1.66	0.90	15.70	0.52	0.95	11.37	0.83	0.98	13.32	0.35	0.97
	BATS	38.29	−10.26	0.78	36.59	9.70	0.73	37.48	−9.14	0.85	19.69	−0.30	0.97

ficient (adopted from the National Center for Atmospheric Research Community Climate Model Version 2) was replaced with that from the new version of SNTHERM (and SAST). However, the original BATS drag coefficient scheme was tested and the results (not shown) were not as good as those shown in Figs. 2–3. Figures 4a,b show that the thermal condition of the atmosphere boundary layer over snow could change dramatically within a day. There was no regular diurnal cycle in the drag coefficient; however, around noon, when the temperature difference between air and land reached a maximum, the atmospheric boundary layer became quite stable, and the drag coefficient approached its minimum value of zero. When temperature differences were small, such as on DOY 124 and DOY 126, the atmospheric boundary layer had neutral stability, and the drag coefficient approached the neutral value. During the snowmelt period, the atmospheric boundary layer was mostly in a very stable condition, which depressed the surface exchanges (Fig. 4c), even though the temperature difference was large (such as on DOY 129). Drag coefficient values calculated in BATS varied in the same direction as that of SNTHERM, but the variations were smaller in magnitude (Fig. 4a).

2) SIGNIFICANCE OF ICE, LIQUID WATER, AND WATER VAPOR FOR SNOWMELT

SNTHERM results were used to compare the amount of energy delivered by the three water phases through their transfer and transport processes. Because a large number of snow layers were used in the SNTHERM simulation and the layer division was varied from time to time, for simplicity these layers were integrated into three layers corresponding approximately to the three layers used in SAST. The net heat fluxes provided by individual water phases to the middle layer (about 2 cm below the snow surface, with a thickness of around 18 cm) were plotted in Fig. 5. Notice two features. First, the energy transfer into or out of the layer by vapor flow was a small fraction of the energy delivered by the liquid water flow and ice conduction. Therefore, the impact of vapor in transferring energy is considered to be unimportant in a simplified snow model. In SNTHERM, the water vapor affects the variation of ice-grain size; therefore, in SAST which neglects the vapor phase, ice-grain size is parameterized as a function of snow density. Second, the heat transfer processes involving both liquid water and ice exhibited strong diurnal characteristics.

According to SNTHERM, the liquid water in the middle layer comes from the top layer and from snowmelt in the layer itself. The inflowing meltwater brings mass and energy into the layer. The liquid water in the layer will refreeze and release latent heat to raise the temperature of the snow layer if the original snow temperature is lower than the melt point; or it will remain partially in the layer and partially flow to the underlying layer (gravitational flow) if the temperature is at the melt point. Figure 5 shows that heat transfer of liquid water occurred in daytime and possessed two stages. First, inflow exceeded outflow and energy accumulated in the layer, reaching a peak around noon (positive portion); then, outflow exceeded inflow and the layer lost energy to the underlying layer (negative portion). From the time series, note that, in the early period of snowmelt (before DOY 128), the energy transmitted into the layer by liquid water was larger than that transmitted out of the layer; thus, the net heat flux of liquid water for the layer was positive. Afterward (DOY 128–136), the energy fluxes approximately balanced, and, later (after DOY136) the energy outflow became dominant and the net heat flux was negative for the layer. Therefore, the liquid water flow acts to transmit solar energy absorbed in the top layer(s) to the deeper layer(s).

In contrast, heat conduction of ice in the middle layer was more important in the evening (Fig. 5, solid line) and mostly had negative (loss) values. In Fig. 6, the simulated temperature profiles of the snowpack at midnight and noontime on DOY 127 are illustrated. Because

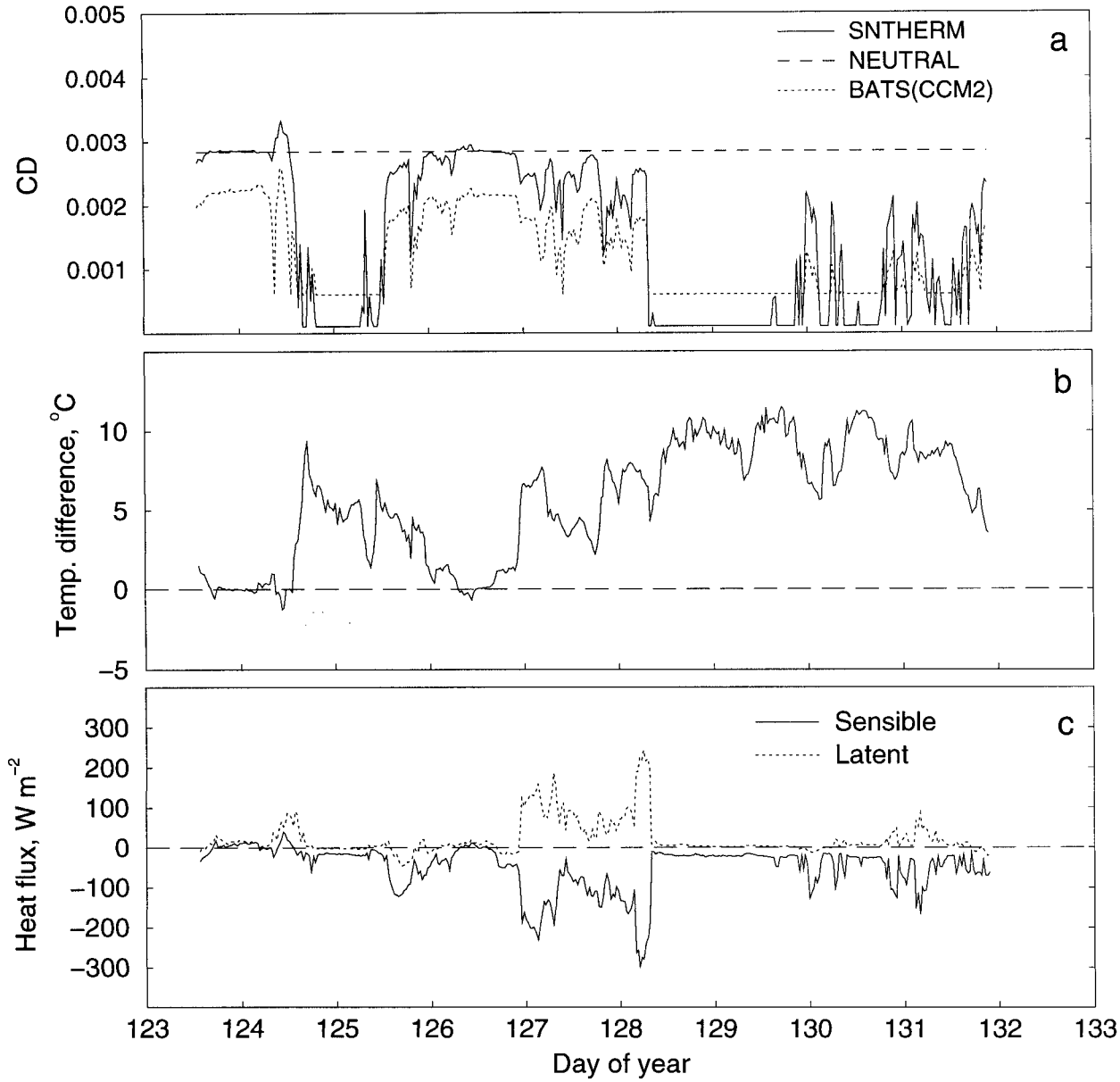

FIG. 4. Hourly time series during DOY 124–131 for (a) drag coefficient, (b) difference between air temperature and snow surface temperature calculated from SNTHERM, and (c) surface sensible and latent heat fluxes calculated from SNTHERM (positive for upward) coefficient as functions of the Richardson number in SNTHERM and BATS (CCM2) calculations.

there was no significant vertical temperature gradient in the daytime (the entire snowpack was at the melting point), no heat was conducted in the snowpack; however, in the evening, the snow surface was refrozen, largely due to the cooling of longwave emission. This resulted in an upward temperature gradient along the snow depth; hence, the ice heat conduction was constantly upward from the lower layer to the upper layer. The evening temperature profiles also indicated that the ice heat conduction was limited to the top region of the snowpack. Note that the SAST model, although using only three vertical layers, provided the same temperature profiles simulated by SNTHERM with a large number of layers (Fig. 6).

3) VARIABILITY OF SNOW DENSITY

The representation of snow density directly changes the snow depth calculations and affects many physical and thermal features of snow, such as liquid water permeability, ice thermal conductivity, and radiation absorption. When using BATS for the Mammoth Mountain simulations, we found that, in order to obtain the good results shown in Figs. 2 and 3, the maximum effective

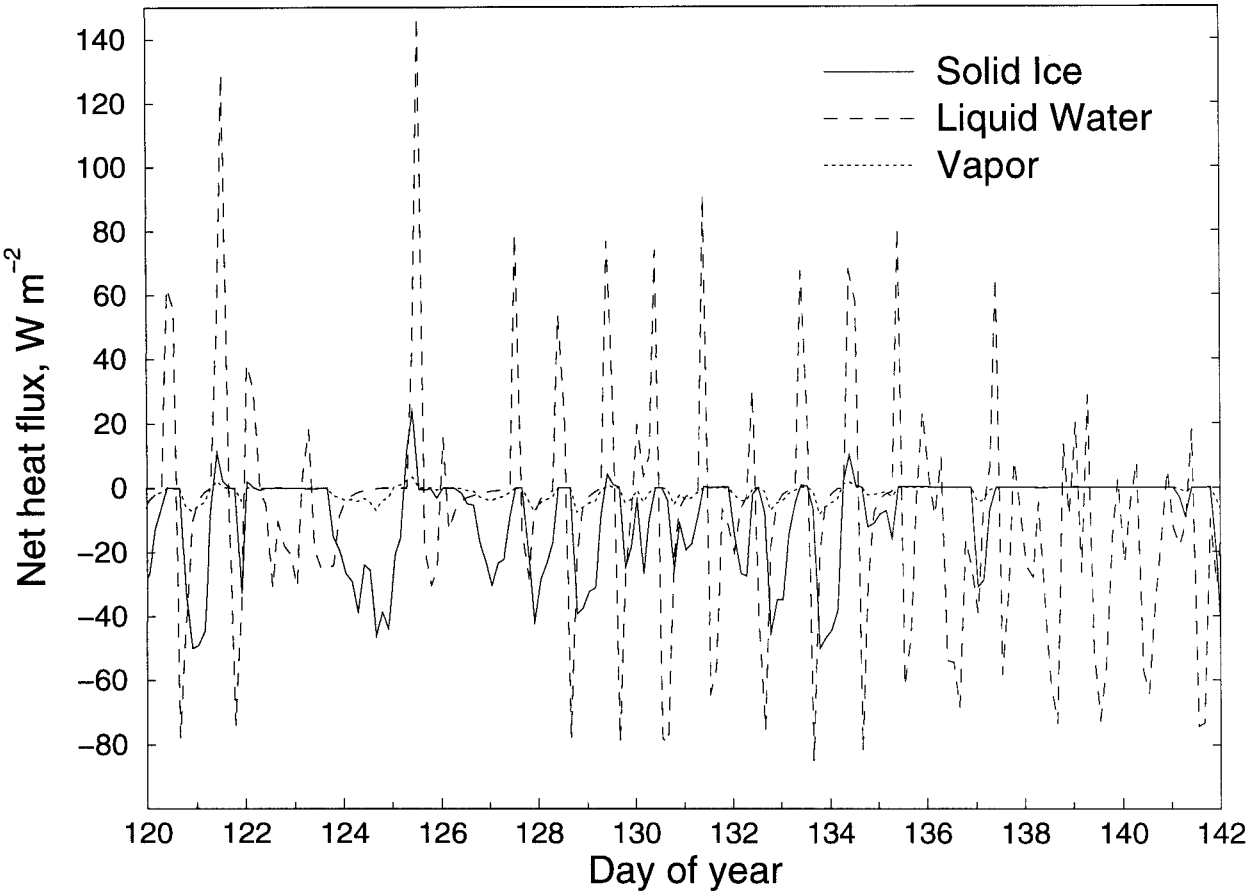

FIG. 5. Hourly time series of the energy gains for the middle layer due to ice conduction, liquid water, and vapor transport. The data were simulated by SNTHERN but integrated according to the three layers used in SAST.

density of snow in the density formula needed to be adjusted from the original setting of 400 kg m^{-3} to 500 kg m^{-3} [cf. Eq. (7) in Yang et al. 1997].

The Mammoth Mountain data provided observations of snow density profiles during the melt season. In Fig. 7, the sample profiles simulated by SNTHERM agree with the observations. Except for the short-range density perturbations along the snowpack (mostly caused by the snowfall history during the season), in general, the snow density profiles were characterized by four regions of variation: (a) in the top (surface to around 20-cm depth), there was a low snow density zone caused by the loss of meltwater and small compaction; (b) in the main body of the snowpack, there was a gradual increase in density along the depth resulting from the snow compaction of weight; (c) in the lower part of the snowpack, a sharp density decrease sometimes developed in the early snowfall because the large temperature gradient in late autumn and early winter might result in faceted grains and a less cohesive and less dense snow (Colbeck 1986); and (d) finally, at the bottom of the snowpack, there often existed high-density slush.

In BATS, snow density is described as the snowpack effective density and varied with snow age. Figure 7 shows that BATS (dotted line) underestimated the density in the simulations. For SAST, two procedures are considered necessary to improve the density simulation: (a) set the total depth of the top two snow layers close to the high-variation zone (top 20 cm) to simulate the transfer from the top low-density zone to the main body compaction zone; and (b) include melting compaction in addition to the weight and metamorphism compaction. Figure 7 shows that, with these two procedures, the density profiles provided by the three-layer SAST model sketched out the two increasing features of snow density profiles, but were unable to capture the low part and bottom features, which were considered less important for snowmelt modeling.

4) DIURNAL FEATURES OF SURFACE TEMPERATURE

The diurnal features of snow surface temperature simulated by the three models are illustrated in Fig. 8. When snow was melting, mostly in the daytime, the surface temperature was fixed at the melting point (0°C). In the evening, when the snow surface was frozen, the tem-

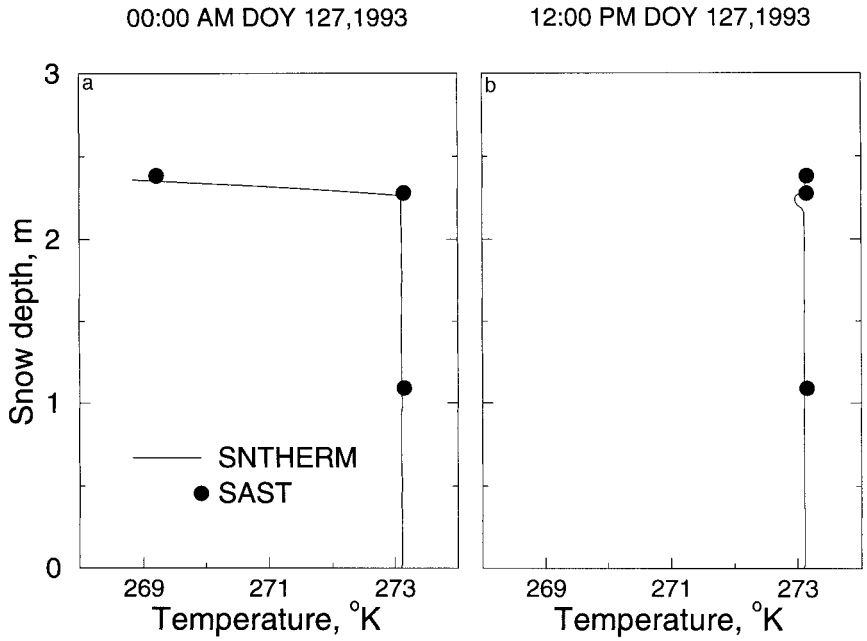

FIG. 6. Snapshots of snow temperature profiles simulated by SNTHERM and SAST: (a) at 0000 LT, DOY 127, 1993, and (b) at 1200 LT, DOY 127, 1993.

perature was below the melting point. The snow surface temperature of BATS had a negative (lower) systematic bias in comparison to the results of SNTHERM, while the SAST-simulated temperature had a positive bias. Figure 8 shows that the bias came from the simulated evening temperature. Two factors were found to have strong influences on the surface temperature calculation: (a) the amount of liquid water in the surface layer (releasing latent heat through freezing and thawing); and (b) the snow density (affecting the heat conduction from the underlying snow layer). In the evening, the daytime meltwater refreezes and releases latent heat to resist the

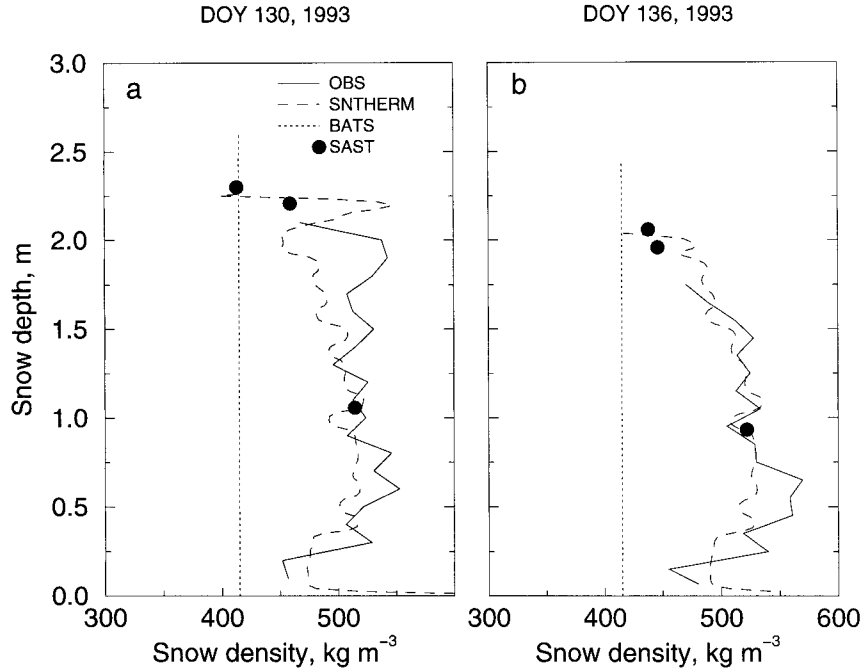

FIG. 7. Comparison of modeled and observed snow density profiles at the north site: (a) at 1400 LT, DOY 130, 1993, and (b) at 1400 LT, DOY 136, 1993.

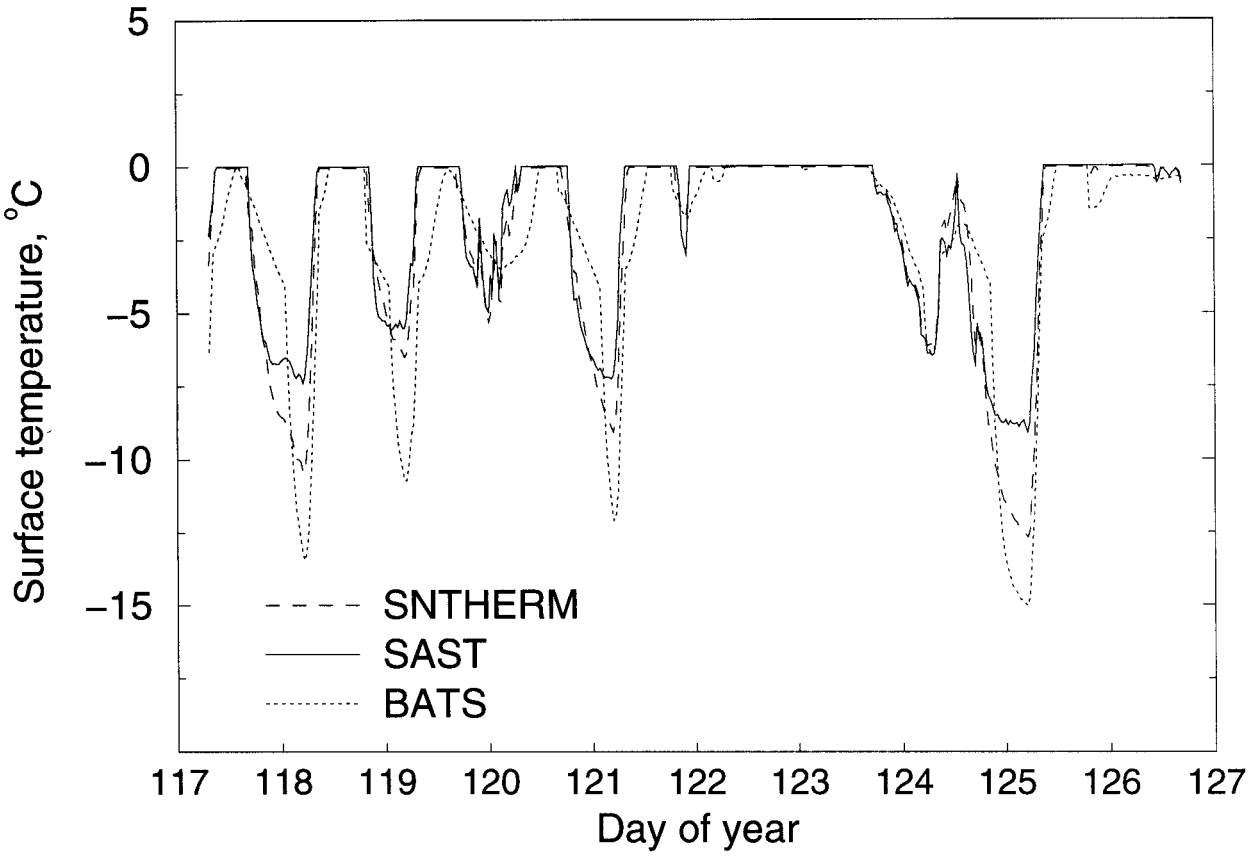

FIG. 8. Diurnal variations of surface temperature simulated by SNTHERM, SAST, and BATS.

decrease in temperature. On the other side, the ice thermal conductivity varies proportionally with the square of snow density. In BATS, because the effect of liquid water was neglected, the heat gain due to the refreezing of meltwater was missing, and the snow density was underestimated, which resulted in less upward heat conduction from deep snow to increase the surface temperature. Therefore, in the evening, snow temperature was lower than that of SNTHERM. In SAST, the nighttime surface temperature was overestimated, mainly because of the parameterization of liquid-water-holding capacity [changing between 5% and 30% as a function of snow density (Loth and Graf 1998a,b)]. Sensitivity tests (results not shown) indicate that, if the liquid-water-holding capacity in SAST is set to zero, the snow surface temperature in the evening will be similar to that of BATS. The systematic bias in snow surface temperature further results in the biases in sensible heat and latent heat flux in the evening. For example, the lower surface temperature causes higher downward sensible heat flux and more condensation.

6. Discussion

In SNTHERM, a large number of layers were used to simulate a snowpack. For better understanding of the physical processes inside a snowpack, the average profiles of eight variables calculated by SNTHERM are plotted (Fig. 9), that is, solar radiation, heat conduction of ice, heat flux of liquid water flow, transform rate from liquid water to ice, temperature, density, porosity, and thermal conductivity. Because of the downward movement of the snow surface during the snowmelt season, the average was calculated from the snow surface downward to the depth of 1.5 m in the snowpack. The average time period was from DOY 109 to DOY 143. Figure 9 indicates that the major changes of most physical variables and parameters took place within the top 20-cm zone; below 20 cm, the variations were more gradual. In particular, the solar radiation and transform rates from liquid water to ice were approximately zero below 9 cm from the surface. We also found that, during the snowmelt period, the heat flux at the snow–soil interface was only about 1 W m^{-2} in the simulations of SNTHERM and SAST (BATS does not explicitly describe the heat flux at the snow–soil interface). Based on these results, in the SAST model, we suggest using a minimum of three layers to represent a thick snowpack, that is, snow depth greater than 40 cm. The thickness of the top layer should be 2 mm to 2 cm, automatically determined by the algorithm; the bottom of the middle layer set at the 20-cm depth; and the re-

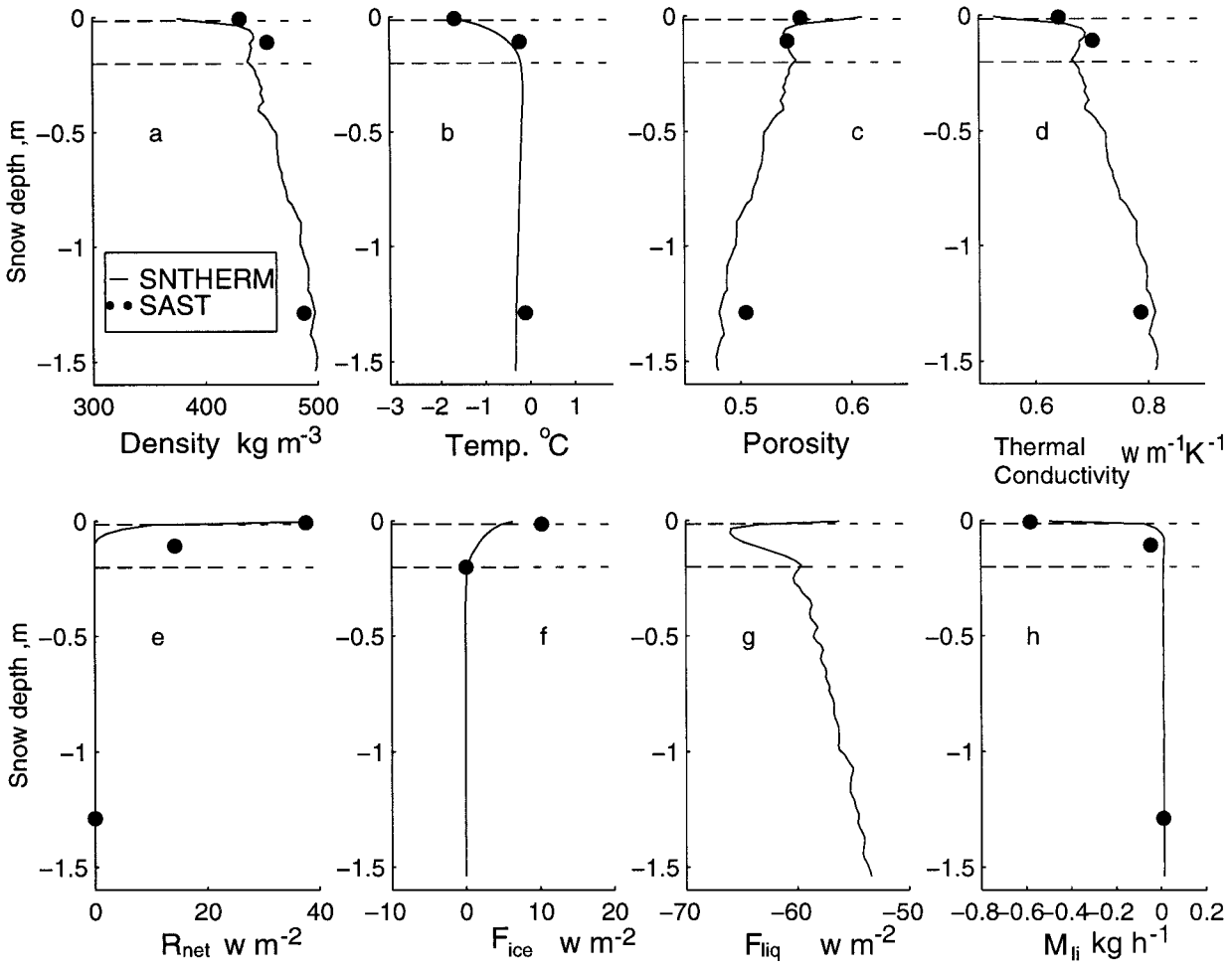

FIG. 9. Averaged profiles of physical variables and parameters calculated by SNTHERM and SAST for (a) snow density, (b) temperature, (c) porosity, (d) thermal conductivity, (e) net solar radiation (R_{net}), (f) heat conduction (F_{ice}), (g) heat flux by liquid water (F_{liq}) (not available in SAST), and (h) transformation rate between liquid water and ice (M_{li}) (positive is liquid water to ice). Because of the movement of the snow surface, only the top 1.5 m of the snowpack is shown. Values represent averages for DOY 109 to 143.

maining part is the bottom layer. The results of SAST using this division are shown in Fig. 9 (circles). Because of the simplifications made in SAST, the current computation of SAST is about 1.8 times that of BATS, and the time step can be fixed at 0.5 h.

From Table 3, checking all six test variables, both SAST and BATS are found to be highly correlated to SNTHERM and possess small rmsd in their seasonal performances. Relatively small but opposite systematic biases were discovered in snow depth, surface temperature, and latent heat flux for BATS and SAST, respectively. In general, SAST results were closer to those of SNTHERM than BATS. However, for long-term (seasonal and annual) performances, the results of SNTHERM do not show significant improvements over those of BATS for the six variables.

The energy transfer processes at the snow surface show strong diurnal variability during the snowmelt seasons—absorbing solar radiation and melting in the daytime, and longwave cooling, refreezing, and ice conduction in the evening. Because the daytime surface temperature is kept at the melting point if the snow surface is melting, the simulation of the three models showed no great difference; however, if the snow surface refreezes during the evening, BATS underestimated surface temperature, thereby resulting in more downward surface latent heat (condensation) and sensible heat flux.

The small biases in BATS-simulated seasonal surface temperature and energy exchanges resulted from neglecting the liquid-water phase in the snow medium and underestimating the snowpack density. These factors affected the manner of energy transfer during the evenings when liquid water in the snow surface was refrozen. The SAST model uses the liquid-water-holding capacity of a snow layer to replace the liquid flow simulated in SNTHERM, which maintains the effects of liquid water on snowmelt energy transfer and saves computation; however, the surface temperature and water discharge simulation were sensitive to the accuracy of the param-

eterization of the holding capacity as a function of snow density.

7. Conclusions

Without any adjustment in model parameters, SNTHERM gave the best agreement with the field observation data for all four test cases in both seasonal and diurnal periods. However, the BATS snow submodel, the simplest one in the three models, also performed well for seasonal periods. It captured the processes that are most important in the top portion of a snowpack where solar radiation provides the major energy source. For snowmelt modeling within GCMs, in which high uncertainties in radiation, precipitation, and other meteorological variables need to be reduced through multiyear averaging of simulation results before making climate analyses, a simple snowmelt model like BATS can provide satisfactory results. The more-involved SNTHERM model captures many physical details that are not represented in the BATS snow submodel, especially the diurnal and vertical variations in snowmelt, which can be crucial to weather, meteorological, and hydrologic studies. The test of SAST indicated that, however, with proper selection of layer depths, a model such as SAST with at least three layers and simpler physical processes than SNTHERM (thereby, inexpensive computation) can yield diurnal and vertical characteristics of snowmelt similar to those shown by SNTHERM.

Heat transport by meltwater and ice and the melt–freeze cycle are crucial to describe the diurnal features of snowmelt physics. Neglect of these processes resulted in underestimation in nighttime surface temperature and biases in sensible and latent heat fluxes. Because the energy delivered through the vapor phase in this snowpack was less than 10% of the energy transmitted by liquid water and ice, water vapor simulation is considered secondary for GCM applications.

This study only examined snowmelt periods using observed net solar and longwave incident radiation. The important effects of snow albedo, vegetation cover, snowfall accumulation, and atmospheric feedback are not tested in this study and should be included in future studies. Copies for SAST codes and description are available from the authors by request.

Acknowledgments. Primary support for this research was provided by NASA/EOS Interdisciplinary Research Programs (NAG53640#1, NAG8-1520, NAGW-2062, U.P.N. 428-81-22, and 429-81-22) and the NOAA GCIP program (NA46GP0247). The senior author, J. M. Jin, would like to thank the World Laboratory, International Centre for Scientific Culture (Switzerland) for selecting him as the first recipient of the John Harshbarger Fellowship. C. A. Schlosser and PILPS central (Australia) provided permission for using the PILPS Phase 2(d) data, Y. Xue and R. F. Harrington gave helpful discussions, and D. K. Braithwaite and J. Broermann provided computer assistance. The careful reading and editing provided by C. Thies improved the manuscript.

REFERENCES

Anderson, E. A., 1976: A point energy and mass balance model of a snow cover. NOAA Tech. Rep. NW519

Barnett, T. P., L. Dumenil, U. Schlese, E. Roeckner, and M. Latif, 1989: The effect of Eurasian snow cover on regional and global climate variations. *J. Atmos. Sci.,* **46,** 661–685.

Bonan, G. B., 1996: A land surface model (LSM version 1.0) for ecological, hydrological, and atmospheric studies: Technical description and user's guide. NCAR Tech. Note NCAR/TN−417+STR, 150 pp. [Available from NCAR, P.O. Box 3000, Boulder, CO 80307-3000.]

Cess, R. D., and Coauthors, 1991: Intercomparison of snow-feedback as produced by general circulation models. *Science,* **253,** 888–892.

Colbeck, S. C., 1986: Classification of seasonal snow cover crystals. *Water Resour. Res.,* **22,** 59–70.

Dickenson, R. E., 1988: The force-restore model for surface temperature and its generalizations, *J. Climate,* **1,** 1086–1097.

——, A. Henderson-Sellers, P. J. Kennedy, and M. F. Wilson, 1986: Biosphere Atmosphere Transfer Scheme (BATS) for the NCAR Community Climate Model. NCAR Tech. Note NCAR/TN−275+STR, 69 pp. [Available from NCAR, P.O. Box 3000, Boulder, CO 80307-3000.]

——, ——, and ——, 1993: Biosphere Atmosphere Transfer Scheme (BATS) version 1e as Coupled to the NCAR Community Climate Model. NCAR Tech. Note NCAR/TN−387+STR, 72 pp. [Available from NCAR, P.O. Box 3000, Boulder, CO 80307-3000.]

Douville, H., J.-F. Royer, and J.-F. Mahfouf, 1995: A new snow parameterization for the Meteo-France climate model. Part I: validation in stand-alone experiments. *Climate Dyn.,* **12,** 21–35.

Foster, J., G. Liston, R. Koster, R. Essery, H. Behr, L. Dumenil, D. Verseghy, S. Thompson, D. Pollard, and J. Cohen, 1996: Snow cover and snow mass intercomparisons of general circulation models and remotely sensed datasets. *J. Climate,* **9,** 409–426.

Hardy, J. P., R. E. Davis, R. Jordan, X. Li, C. Woodcock, W. Ni, and J. C. McKenzie, 1997: Snow ablation modeling at the stand scale in a boreal jack pine forest. *J. Geophys. Res.,* **102,** 29 397–29 405.

Harrington, R. F., and R. C. Bales, 1998: Interannual, seasonal and spatial patterns of meltwater and solute fluxes in a seasonal snowpack. *Water Resour. Res.,* **34,** 823–831.

Houghton, J. T., L. G. Meira Filho, B. A. Callander, N. Harris, A. Kattenberg, and K. Maskell, 1996: *Climate Change 1995: The Science of Climate Change*. Cambridge University Press, 572 pp.

Jin, J., X. Gao, S. Sorooshian, Z.-L. Yang, R. Bales, R. E. Dickinson, S. Sun, and G. Wu, 1999: One-dimensional snow water and energy balance model for vegetated surfaces. *Hydrological Processes.*

Jordan, R., 1991: A one-dimensional temperature model for a snow cover. U.S. Army Corps of Engineers, Cold Regions Research and Engineering Laboratory, Special Report 91-16, 49 pp. [Available from CRREL, 72 Lyme Rd., Hanover, NH 03755-1290.]

Leese, J. A., 1997: Major activities plan for 1998, 1999 and outlook for 2000 for the GEWEX Continental-Scale International Project (GCIP). IGPO Publication Series, No. 26, Silver Spring, MD.

Li, X., A. H. Strahler, and C. R. Woodcock, 1995: A hybrid geometric optical-radiative transfer approach for modeling albedo and directional reflectance of discontinuous canopies. *IEEE Trans. Geosci. Remote Sens.,* **33,** 466–480.

Loth, B., and H. F. Graf, 1998a: Modeling the snow cover in climate studies. Part I: Long-term integrations under different climatic

conditions using a multi-layered snow-cover model. *J. Geophys. Res.,* **103,** 11 313–11 327.
——, and ——, 1998b: Modeling the snow cover in climate studies. Part II: Sensitivity to internal snow parameters and interface processes. *J. Geophys. Res.*, **103,** 11 329–11 340.
——, ——, and J. M. Oberhuber, 1993: Snow cover model for global climate simulations. *J. Geophys. Res.*, **98,** 10 451–10 464.
Lynch-Stieglitz, M., 1994: The development and validation of a simple snow model for GISS GCM. *J. Climate*, **7,** 1842–1855.
Marshall, S., J. O. Roads, and G. Glatzmaier, 1994: Snow hydrology in a general circulation model. *J. Climate*, **7,** 1251–1269.
Pollard, D., and S. L. Thompson, 1995: Use of a land-surface-transfer scheme (LSX) in a global climate model: The response to doubling stomatal resistance. *Global Planet. Change*, **10,** 129–161.
Rowe, C. M., K. C. Kuiven, and R. Jordan, 1995: Simulation of summer snowmelt on the Greenland ice sheet using a one-dimensional model. *J. Geophys. Res.*, **100,** 16 265–16 273.
Schlosser, A. C., A. Robock, K. Y. Vinnikov, N. A. Speranskaya, and Y. Xue, 1997: Eighteen-year land-surface hydrology model simulations for a midlatitude grassland catchment in Valdai, Russia. *Mon. Wea. Rev.*, **125,** 3279–3296.
——, and Coauthors, 1999: Simulation of boreal grassland hydrology at Valdai, Russia: PILPS Phase 2(d). *Mon. Wea. Rev.*, in press.
Sellers, P. J., Y. Mintz, Y. C. Sud, and A. Delcher, 1986: A Simple Biosphere model (SiB) for use within general circulation models. *J. Atmos. Sci.*, **43,** 505–531.
Sun, S. F., J. Jin, and Y. Xue, 1999: A simple snow-atmosphere-soil transfer (SAST) model. *J. Geophys. Res.*, in press.
Tarboton, D. G., and C. H. Luce, 1996: Utah Energy Balance Snow Accumulation and Melt Model (UEB). Computer model technical description and user's guide. Utah Water Research Laboratory and USDA Forest Service Intermountain Research Station. [Available from Civil and Environmental Engineering, Utah State University, Logan, UT 84322-4110.]
Verseghy, D. L., 1991: CLASS—A Canadian Land Surface Scheme for GCMs. Part I: soil model. *Int. J. Climatol.*, **11,** 111–133.
Walland, D. J., and I. Simmonds, 1996: Sub-grid-scale topography and the simulation of Northern Hemisphere snow cover. *Int. J. Climatol.*, **16,** 961–982.
——, and ——, 1997: Modelled atmospheric response to changes in Northern Hemisphere snow cover. *Climate Dyn.,* **13,** 25–34.
Wu, G. X., J. S. Xue, Z. Z. Wang, H. Liu, A. G. He, and Y. C. Zhao, 1995: The impacts of the snow-melt timing of the Tibetan Plateau on the seasonal variation in Southern China (in Chinese). *Gansu Meteor.*, **13,** 1–8.
Yang, Z.-L., R. E. Dickinson, A. Robock, and K. Y. Vinnikov, 1997: Validation of the snow sub-model of the Biosphere-Atmosphere Transfer Scheme with Russian snow cover and meteorological observational data. *J. Climate,* **10,** 353–373.
Yasunari, T., A. Kitoh, and T. Tokioka, 1991: Local and remote responses to excessive snow mass over Eurasia appearing in the northern spring and summer climate—A study with the MRI GCM. *J. Meteor. Soc. Japan,* **69,** 473–487.
Yeh, T.-C., R. T. Wetherald, and S. Manabe, 1983: A model study of the short-term climate and hydrologic effects of sudden snow-cover removal. *Mon. Wea. Rev.*, **111,** 1013–1024.